

## **Design and Characteristic Analysis of Skeleton type Single-Phase Brushless DC Motor Using Finite Element Method**

Yang-Su Lim, Kyung-Ho Ha, Jeong-Jong Lee, Jung-Pyo Hong, Senior Member, IEEE

Y. S. Lim is with the Automotive Motor Division at Daewoo Precision Industries Co. LTD, Kumjeong, Busan, 609-600 P.O.BOX 25, Korea, yslim@dpi.daewoo.co.kr

K. H. Ha is with the POSCO, Pohang, Gyeongbuk, 790-785, Korea, khha@posco.co.kr

J. J. Lee and J. P. Hong are with the Department of Electrical Engineering at Changwon National University, Changwon, 641-773, Kyungnam, Korea, wave95@orgio.net; jphong@sarim.changwon.ac.kr

*Abstract--This paper deals with the design of Skeleton type single-phase Brushless DC motor (SBLDC) to overcome its drawbacks. The design aspect is to eliminate the dead zone that can lead to a starting problem, protect the inflow of dust through the link part and even increase the performance. If the link is closed to protect the dust, this structure produces a distorted back-emf. Thus, to solve these problems, a stator core with a asymmetric airgap and a closed link is proposed. The characteristics are calculated by 2D finite element method (FEM) coupled with circuit equations. It is proved by experimental results.*

### **I. Introduction**

SINGLE-PHASE motors are widely used in industrial and household applications. The reason is that the operation is fed directly from a commercial single-phase voltage source. Facing the rising cost of electric energy, consumers and manufactures have paid much attention to energy saving in an attempt to reduce their operating costs. These requirements are mainly achieved by choosing a proper single-phase motor and optimizing the motor design. The SBLDCs in single-phase motors has substituted single-phase induction motor with shaded poles because the latter have low efficiency characteristics. SBLDCs have many advantages in economical efficiency that means simple motor construction and low cost driver topology with only two power switches. These characteristics are competent to satisfy the demands for a part of household electric appliances.

A general SBLDC has zero torque zones, i.e. dead zones, which can lead to starting problems. In addition, it has an open link in the stator core, as shown in Fig. 1, to prevent the leakage flux driven by the permanent magnet passing the link. If the link is closed to prevent a lock of the rotor due to the inflow of dust, the back-emf is distorted and the performance is deteriorated. Therefore, the link and the detent groove in the stator core are very important design parameters to solve these problems. These parameters have influence on the torque profile, such as torque ripple and reverse torque zone, so that the investigation of these parameters is needed [1].

This paper proposes a improved stator core that is very effective to solve the above problem. The function of the detent groove is to produce a cogging torque, which is used for the reduction of the dead zone. From the analysis results, the optimal detent groove is determined; further - the link is closed to protect the inflow of dust while preserving the magnetic torque requirement. For the stator core design, the dynamic characteristics considering instantaneous current caused by the nonlinear inductance varying with rotor position is calculated by 2D finite element method (FEM) coupled with circuit equations. Some measurements and computation results of the improved model are compared with those of the conventional model.

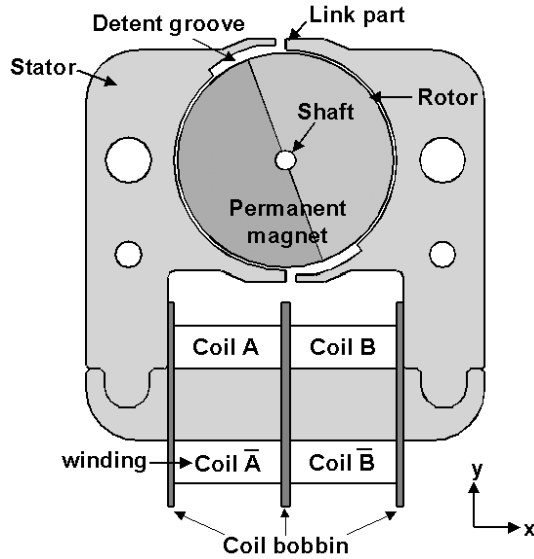


Fig. 1 Configuration of the skeleton type single-phase BLDC motor

TABLE I. Specifications of The Motor

Design parameter	Design parameter value	Design parameter	Design parameter value
Input AC voltage (V)	220	Rated speed (rpm)	2200
Input frequency (Hz)	50	Operating temperature (°C)	-30
Rated torque (gf-cm)	50	Rated operating efficiency (%)	55 upper

## II. Design Model and Analysis Method

### A. Design Model

A skeleton type single-phase BLDC with a detent groove shape and a link part in the stator core structure is designed as the cooling fan motor for a refrigerator. Fig. 1 shows the configuration of the SBLDC. The inner rotor consists of a ring type permanent magnet and the shaft. The magnetic material is ferrite magnet with a residual flux density of approximately 0.7(T). The shaft also functions as the return path for the magnetic flux. Table I presents the requirement specifications of the SBLDC for driving the evaporator fan.

### B. Design Concept

The stator core of the conventional model has an open link part to reduce the flux leakage driven by the permanent magnet but the motor can be locked due to the inflow of dust through the opened link part, as illustrated in Fig. 2(a). If the link part is closed, the distorted back EMF waveform is generated and the motor characteristics deteriorate. This is due to the increase of flux leakage. A dead-zone, where no torque is developed results, leading to a starting problem. In order to get rid of the dead-zone it is possible to choose a detent groove with an asymmetric airgap. The stator core with a detent groove produces a cogging torque that helps to reduce the dead zone.

This paper proposes a new stator structure to solve the above-mentioned problem. Fig. 2(b) shows the proposed stator core. First, the upper link part is closed and the lower one opened. In the case of the upper link, the minimum flux leakage and the protection of dust are accomplished by the closed link with the very thin structure, as plotted on Fig. 2(b). In the case of the lower link, its aperture is filled with a coil bobbin to prevent the inflow of dust. Next, a proper detent angle and shape is determined from analysis results to increase the starting torque.

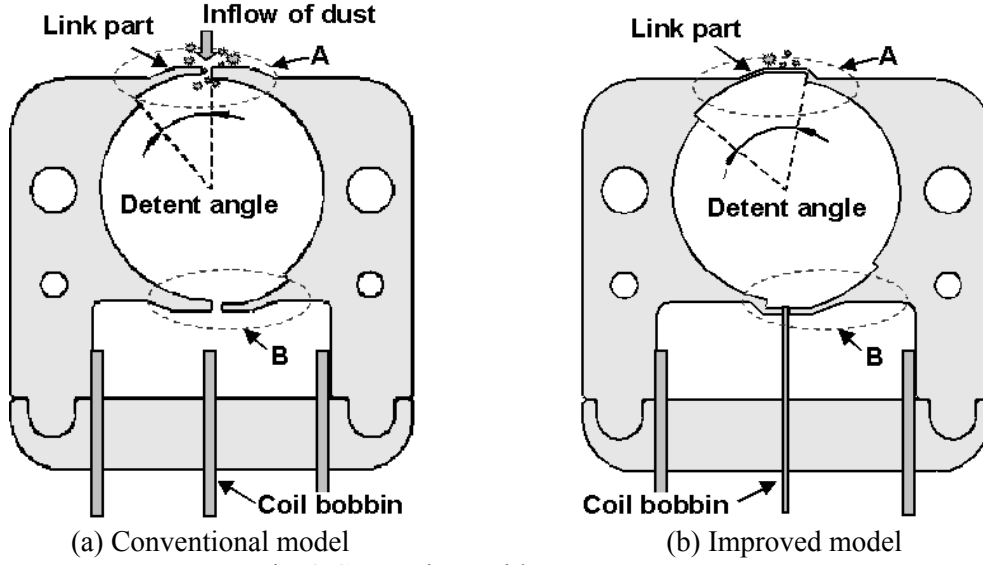


Fig. 2 Comparison with stator core structure

### C. Field Computation Method

The 2D FEM is used to take into account the nonlinear characteristics of the electric machine. The governing equation of the magnetostatic field problem with magnetic vector potential is generally expressed as follows [3]:

$$\nabla \times \frac{1}{\mu} (\nabla \times \mathbf{A}) = \mathbf{J}_0 + \mathbf{J}_m \quad (1)$$

$$\mathbf{J}_m = \frac{1}{\mu_0} \nabla \times \mathbf{M} \quad (2)$$

where  $\mathbf{A}$  is the magnetic vector potential,  $\mathbf{J}$  is the applied current density,  $\mathbf{J}_m$  is the magnetized current density,  $\mathbf{M}$  is the magnetization,  $\mu_0$  and  $\mu$  are the magnetic permeability in vacuum and core, respectively.

The detailed performance study of the SBLDC requires an analysis considering its controller. For the analysis of the dynamic characteristics, a voltage equation is coupled with equation (1) and then the system matrix is obtained by time difference schemes. The voltage equation of one phase of SBLDC is as follows:

$$V_s = R_m i_m + L_m \frac{di_m}{dt} + E_m \quad (3)$$

where  $V_s$  is the supply voltage,  $R_m$  is the winding resistance per phase,  $i_m$  is the phase current,  $L_m$  is leakage inductance of end-coil and  $E_m$  is back-electromotive force induced in the coil[4].

### D. Calculation of Torque

The method of the Maxwell stress tensor is used to calculate the static torque for the rotor position. The torque is given by the following equation (4).

$$\mathbf{T} = \oint_s \mathbf{r} \times \mathbf{P} dS \quad (4)$$

where  $\mathbf{r}$  is the distance vector of a point to axis rotation.

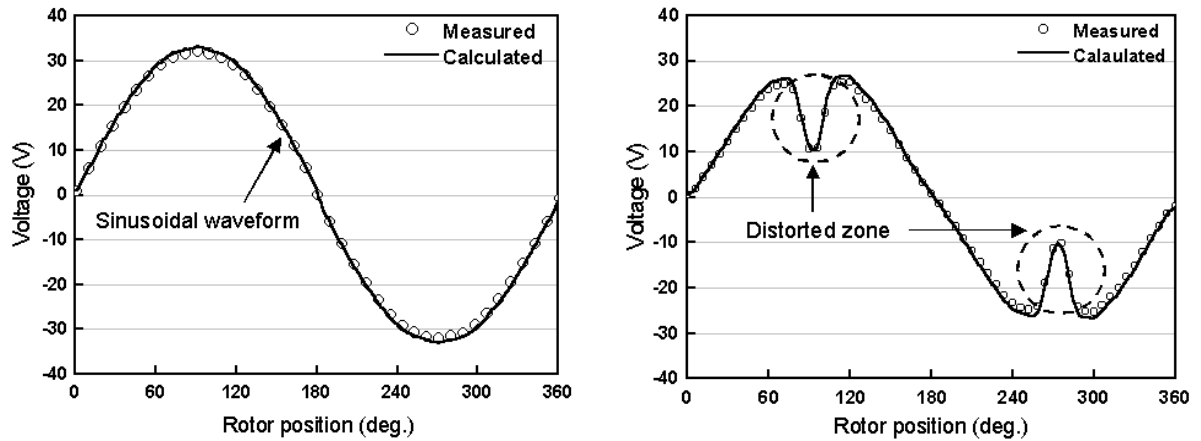
Equation (4) is obtained by the surface integration of a stress tensor vector  $\mathbf{P}$  over an air gap enclosing the rotor surface  $\mathcal{S}$ . Maxwell stress tensor is given by (5)[5].

$$\mathbf{P} = \frac{1}{\mu_0}(\mathbf{n} \cdot \mathbf{B})\mathbf{B} - \frac{1}{2\mu_0}\mathbf{B}^2\mathbf{n} \quad (5)$$

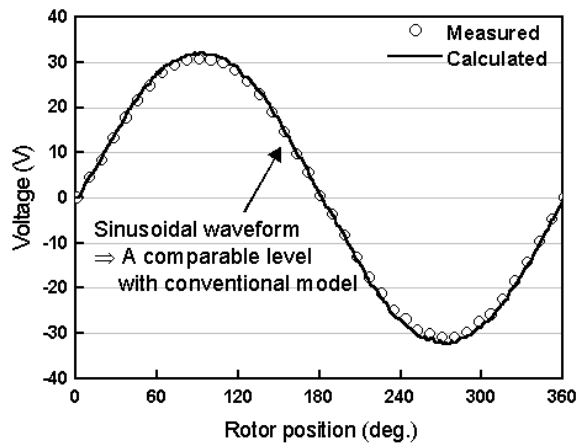
where  $\mu_0$  is the permeability of free space,  $\mathbf{n}$  is the direction of the normal unit vector on the surface  $\mathcal{S}$ ,  $\mathbf{B}$  is the flux density solved by electromagnetic FEM.

### III. Design and Analysis Results

Fig. 3 shows the comparison of the back-emf waveforms for the each mode when the rotor rotates at 2000(rpm). The conventional model with an open link, as shown in Fig. 3(a), gives the sinusoidal back-emf waveforms. This model has a disadvantage of the inflow of dust through the opened link part, so the link part should be closed. In contrast to this model, the conventional model with the closed link produces the back-emf waveform distorted by the flux leakage, as presented on Fig. 3(b). Therefore, the thickness of closed link in the improved model is designed as 0.5(mm) considering the manufacturing of wire cutting and the mechanical strength. The back-emf of the new model, as opposed to the conventional model with an open link, is improved. In Fig. 3(c), the improved model generates a sinusoidal back-emf, which is similar to that of conventional model with the opened link. The analysis results for all models are similar to the measurements. In this way, the calculation program used in this study is suitable to design the stator core.



(a) Conventional model with the opened link part (b) Conventional model with the closed link part



(c) Improved model

Fig. 3 Back-emf waveforms for the each model

On the other hand, the detent groove angle is determined to solve the starting problem and improve the resultant torque. For a parametric study of the detent angle, the model has a closed link of 0.5(mm) thickness. Fig. 4 shows the variation of cogging torque and the resultant torque for the detent angle. In Fig. 4, the cogging torque steadily increases by increasing the detent angle because the variation of the permeance in the air gap is increased. The phase of the cogging torques is also changed. The detent angle has an effect on the magnitude and phase of cogging torque. Fig. 5 shows the resultant torque versus the detent angle. The resultant torque is the sum of the cogging torque and the magnetic torque resulting from the phase current. The resultant torque increases until detent angle of 61(deg.) and decreases there after. This observation leads to a conclusion that the detent angle of 61(deg.) is the most suitable for increasing the resultant torque. The resultant torque meets the demand level. Fig. 6 shows the resultant torque, cogging torque and magnetic torque at a detent angle of 61(deg.). The magnetic torque generates dead zones at 0 and 180(deg.). However, the dead zones in the resultant torque disappeared with the help of the cogging torque. Finally, we determine that the improved model have the thin closed link and the detent angle of 61(deg.)

The experimental results of two models at the fan load, the conventional model with the opened link and the improved model, are shown in Table II. The motor volume is restricted by the space of system. The AC supply voltage is converted into a DC voltage by the driver. The performance of the improved model is identical to that of the conventional model with the open link of the same dimension. The improved model can protect the inflow of dust due to the closed link.

Fig. 7 shows the speed versus the resultant torque. The measured characteristic curve of the improved model matches that of the conventional model with the opened link. Fig. 8 is the picture of the fabricated motor with its drive.

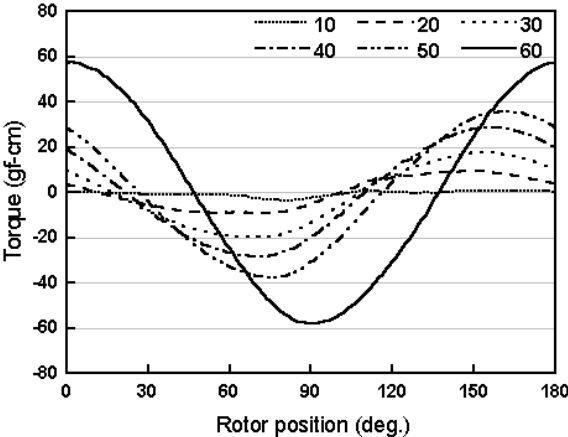


Fig. 4 Cogging torque characteristics according to the detent angle

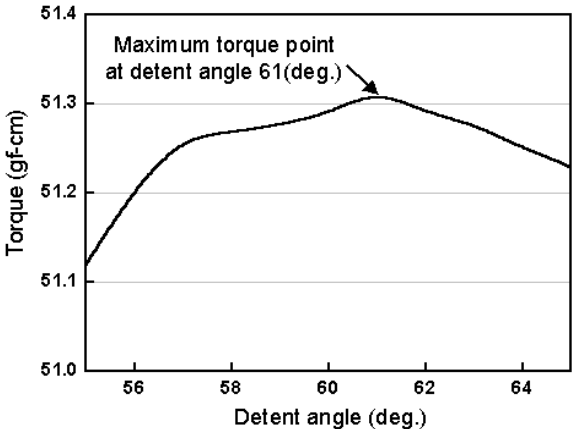


Fig. 5 Resultant torque according to the detent angle

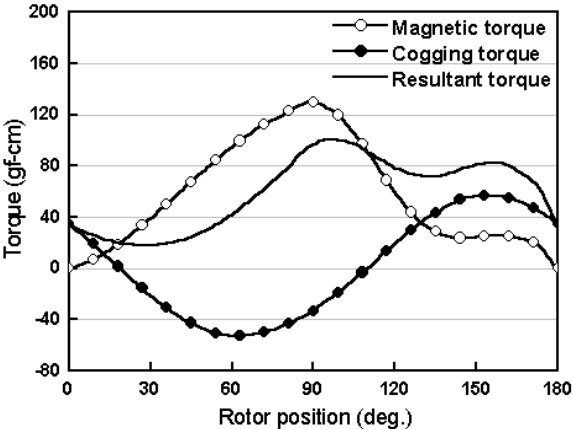


Fig. 6 Torque profile of the improved model

## IV. Conclusion

This paper studies the effect of stator core structure on torque characteristics for the SBLDC design. From the results, the improved stator structure is proposed to protect the inflow of dust, to remove dead zones and even to increase resultant torque. Its upper and lower link is closed and opened, respectively. An optimal detent groove angle is determined. Therefore, it is expected that the proposed stator structure design can be easily utilized to solve the above-mentioned problem.

### References

- [1] S. Bentouati, Z. Q. Zhu, D. Howe, "Influence of design parameters on the starting torque of a single-phase PM brushless DC motor," *IEEE Tans. on Magnetics*. Vol.36, No.5, pp3533-3536, 2000.
- [2] J.R. Hendershot Jr., Timothy J. E. Miller, *Design of Brushless Permanent-Magnet Motors*, Magna Physics Publishing and Clarendon Press, 1994.
- [3] S. J. Salon, *Finite element analysis of electrical machines*, Kluwer academic, London, UK, 1995
- [4] S. C. Park, T. H. Yoon, B. Y. Yang, B. I. Kwon and Y. S. Jin, "Finite Element Analysis of a Two-Phase Brushless Motor," *Small Motors & Servo Motors International Conference - SMIC '99 TOKYO*, pp.305-308, 2000.
- [5] M. J. DeBortoli and S. J. Salon, "Computation of forces and torque in electromagnetic devices using the finite element method," *International Conference on Electrical Machines*, pp. 699-705, 1990.

Table II. Comparison of experimental results for two models

Parameters	Conventional model with the opened link	Improved model
Supply voltage (V)	220	220
Input frequency (Hz)	50	50
Rated speed (rpm)	2280	2300
Rated torque (gf-cm)	50.1	50.1
Stator size (mm)	61×60×Φ34×11.5	61×60×Φ34×11.5
Back-emf (V <sub>rms</sub> /krpm)	9.6	9.5
Efficiency (%)	55.8	55.2

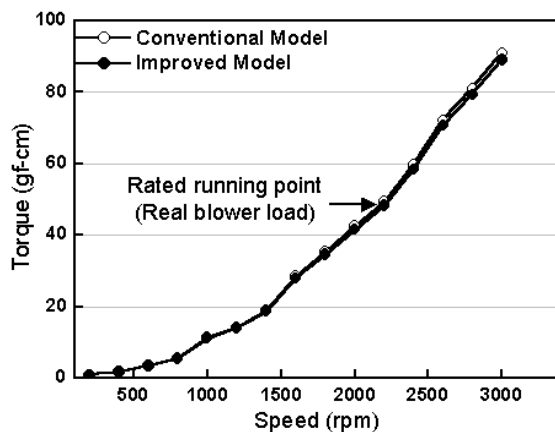


Fig. 7 The measured characteristic curve

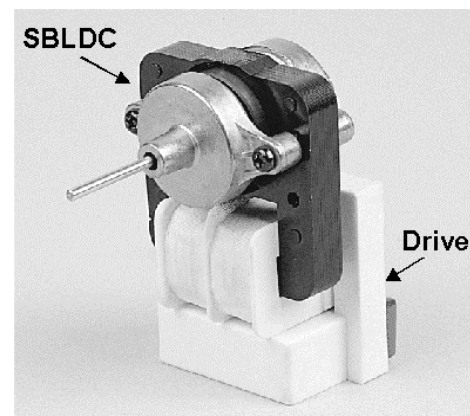
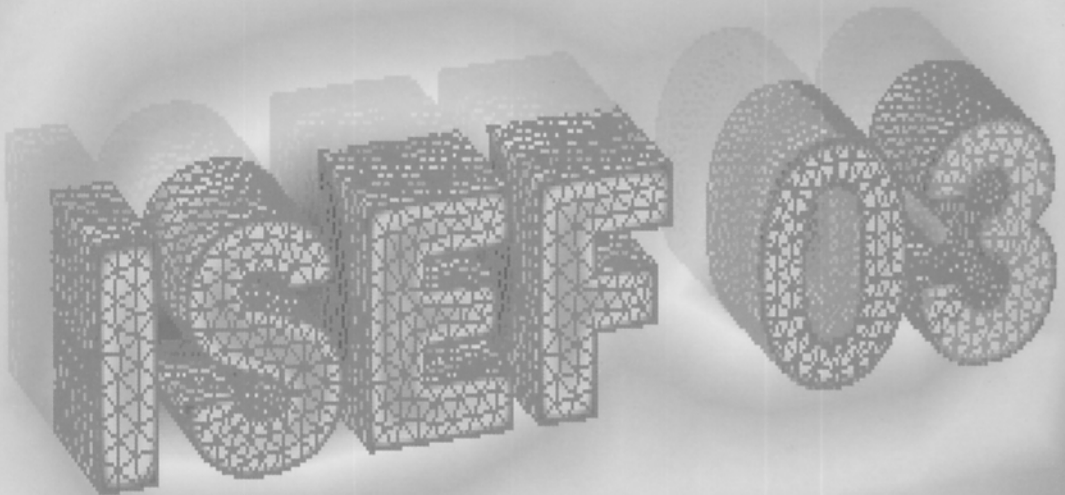


Fig. 8 The improved SBLDC with its drive



XI INTERNATIONAL SYMPOSIUM  
ON **ELECTROMAGNETIC FIELDS**  
IN ELECTRICAL ENGINEERING  
**ISEF 2003**



SEPTEMBER 18-20, 2003

MARIBOR, SLOVENIA

**The Symposium is organised by:**

- Research group Applied Electromagnetics, Faculty of Electrical Engineering and Computer Science, Maribor, Slovenia
- University of Maribor, Slovenia
- Institute of Mechatronics and Information Systems, Technical University of Lodz, Poland
- Department of Fundamental Research, Electrotechnical Institute, Warsaw, Poland

**VOLUME 1**

7. <b>The Influence of Brush Shift on EMF in Small Commutator Machines</b> M. Klauz, T.JE Miller .....	777
8. <b>An Improved 2-Phase Snail-Cam Type Fan Motor Design</b> J.Y. Lee, G.H. Lee, J.J. Lee, J.P. Hong, K.H. Ha .....	783
9. <b>Design and Characteristic Analysis of Skeleton Type Single-Phase Brushless DC Motor Using Finite Element Method</b> Y.S. Lim, K.H. Ha, J.J. Lee, J.P. Hong.....	789
10. <b>Analysis of Magnetization Characteristics of HTS Bulk Rotor in a Rotating Magnetic Field</b> T. Nakamura, H.J. Jung, N. Tanaka, I. Muta, K. Fukui .....	795
11. <b>The 3D Dynamic Simulation of the Inverter Fed Electromechanical Actuators Including Eddy Currents</b> L. Nowak.....	801
12. <b>Analysis and Design Program of Switched Reluctance Motor Using an Analytical Method</b> P.J. Otaduy, J. McKeever, D. Adams, P.S. Shin.....	805
13. <b>Influence of Machine Symmetry on Cogging Torque in Variable Reluctance Permanent-Magnet Motors</b> H. Öztura .....	811
14. <b>Power Losses Analysis in the Windings of Electromagnetic Gear</b> A. Patecki, S. Stępień, G. Szymański.....	817
15. <b>Evaluation of New Surface Mounted Permanent Magnet Synchronous Machine with Finite Element Calculations</b> T. Schneider, A. Binder.....	823
16. <b>Parameterization Coupling Model of Saturated Linear Synchronous Reluctance Motor and Its Parameters</b> G. Štumberger, B. Štumberger, D. Dolinar.....	829
17. <b>Finite Element Analysis of the Magnetorheological Fluid Brake Transients</b> W. Szeląg .....	835
18. <b>Analysis of Supplementary Conditions for a Smooth Torque Running of Heteropolar Excited Vernier Reluctance Machines</b> S. Taïbi, Th. Henneron, A. Tounzi.....	841
19. <b>Numerical Analysis of the Brushless Motor Magnetic Field and Torque</b> I. Tičar, A. Stermecki, I. Zagradišnik.....	847
20. <b>3-D FEA and Topology Optimization of Linear Motor for Linear Compressor</b> S. Wang, J. Kang, H. Lee, E. Hong, K. Park .....	853
21. <b>Effect of Coil Shapes on Thrust Characteristics of Linear Induction Motor</b> T. Yamaguchi, Y. Kawase, T. Eguchi.....	859
22. <b>Frequency Discriminator Based on Dielectric Resonator and Hybrid Ring</b> E.Y. Yuksel, T.T.Y. Wong.....	863